AIAA JOURNAL
Vol. 37, No. 11, November 1999

Limit Cycle Oscillations of Delta Wing Models in Low Subsonic Flow

Deman Tang,* James K. Henry,† and Earl H. Dowell‡
Duke University, Durham, North Carolina 27708-0300

A nonlinear, aeroelastic analysis of a low-aspect delta wing modeled as a plate of constant thickness demonstrates that limit cycle oscillations (LCOs) of the order of the plate thickness are possible. The structural nonlinearity arises from double bending in both the chordwise and the spanwise directions. The results using a vortex lattice aerodynamic model for a low-Mach-number flow complement earlier studies for rectangular wing platforms that showed similar qualitative results. The theoretical results for the flutter boundary (beyond which LCO occurs) have been validated by comparison to the experimental data reported by other investigators for low-aspect-ratio delta wings. Also, the LCOs found experimentally by previous investigators (but not previously quantified prior to the present work) are consistent with the theoretical results reported here. Reduced-order aerodynamic and structural models are used to substantially decrease computational cost with no loss in accuracy. Without the use of reduced-order models, calculations of the LCO would be impractical. A wind-tunnel model is tested to provide a quantitative experimental correlation with the theoretical results for the LCO response itself.

Nomenclature

a_i, b_j	= generalized coordinates
c	= delta wing root chord
D	= delta wing plate bending stiffness
E	= Young's modulus
h	= delta wing plate thickness
km, kn	= numbers of vortex elements on delta wing
kmm	= total number of vortices on both the delta wing and wake in the x direction
L	= delta wing span
m	= delta wing panel mass/area, $h\rho_m$
mxy	= number of delta wing modal functions in the x and y, plane defining u and v
nxy	= number of delta wing modal functions in the z direction defining w
Q^{ij}	= generalized aerodynamic force
q_n	= generalized coordinate in the z direction
R_a	= size of reduced-order aerodynamic model
R_x, R_y, R_z	= rotatory displacements
t	= time
U	= airspeed
U_f	= flutter airspeed
U_i, V_j	= modal functions in x and y directions
u, v	= in-plane displacements
W_k	= transverse modal function in z direction
w	= plate transverse deflection
$[X], [Y]$	= right and left eigenvector matrices of vortex lattice eigenvalue model
x, y	= streamwise and spanwise coordinates
$[Z]$	= eigenvalue matrix of vortex lattice
z	= normal coordinate
z_i	= discrete time eigenvalue
Γ	= vortex strength
$\underline{\Delta p}$	= aerodynamic pressure loading on panel
Δp	= nondimensional aerodynamic pressure, $\Delta p/(\rho_\infty U^2)$
Δt	= time step, $\Delta x/U$
Δx	= plate element length in the streamwise direction
λ_i	= continuous time eigenvalues, $\ell_n(z_i)/\Delta t$
ν	= Poisson's ratio
ρ_∞, ρ_m	= air and plate densities
τ	= time parameter, $\sqrt{(mc^4/D)}$, s
ω	= frequency
$\cdot$	= d()/dt

Received 29 May 1998; revision received 4 March 1999; accepted for publication 10 March 1999.

*Research Associate, Department of Mechanical Engineering and Materials Science.
†Research Assistant, Department of Mechanical Engineering and Materials Science.
‡J. A. Jones Professor and Dean, School of Engineering.

Introduction

LINEAR and nonlinear aeroelastic responses of panels or plates with fixed supports on all four sides have been studied for many years in flows from subsonic to supersonic.[1,2] More recently plates with free edges have been studied, and these results[3,4] have provided good physical understanding of the flutter and limit cycle oscillation characteristics for such plates in a high-Mach-number supersonic flow. In particular, it has been demonstrated that, even with only a single edge of a plate restrained, bending tension or geometrical nonlinearities can produce limit cycle oscillation amplitudes of the order of the plate thickness. For low subsonic flow speeds, Tang et al.[5] used a three-dimensional time-domain vortex lattice aerodynamic model and reduced-order aerodynamic technique[6,7] to investigate the flutter and limit cycle oscillation characteristics of a cantilevered low-aspect-ratio, rectangular wing–panel structure. Again limit cycle oscillations were found.

Following the work of Ref. 5, in the present paper we also use the vortex lattice aerodynamic model to investigate the flutter and limit cycle oscillation characteristics of a low-aspect-ratio delta wing structure at low subsonic flow speeds. The theoretical results are consistent with the experimental results of Doggett and Solstmann,[8] who previously studied the flutter of low-aspect-ratio delta wings.

To validate the theoretically predicted limit cycle oscillation characteristics of the delta wing, an experimental investigation has been carried out in the Duke University wind tunnel using an Ometron VPI 4000 scanning laser vibrometer system[9] to measure deflections (velocities) of the delta wing. The VPI sensor is a noncontacting transducer that uses optical interferometry and electronic frequency measurements to determine the frequency shift of a beam of light reflected from a moving surface.

State-Space Equations

A schematic of the delta wing–plate geometry with a three-dimensional vortex lattice model of the unsteady flow is shown in Fig. 1. The aeroelastic structure/fluid state-space equations are described as follows.

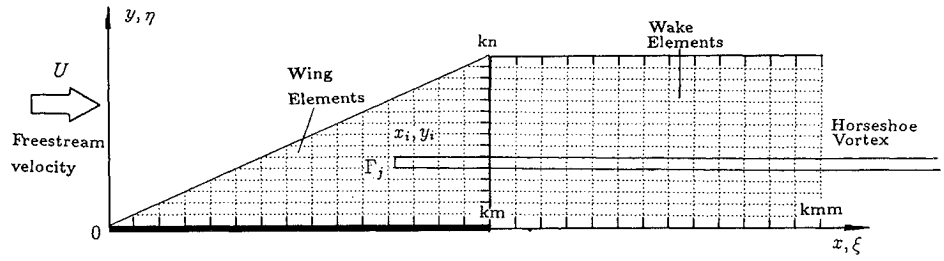

Fig. 1 Aeroelastic model of a delta wing.

Nonlinear Structural Equations

The nonlinear structural equations were derived from the Lagrange equations based on the von Kármán plate equations[1,3,4] using the total kinetic and elastic energies and the work done by applied aerodynamic loads on the plate. Modal expansions for the plate deflection are substituted into the energy expressions and then into Lagrange's equations to yield equations of motion for each structural modal coordinate.

We expand the transverse or out-of-plane displacement w and the in-plane displacements u and v as follows:

$$u = \sum_i a_i(t)U_i(x, y) \tag{1}$$

$$v = \sum_j b_j(t)V_j(x, y) \tag{2}$$

$$w = \sum_k q_k(t)W_k(x, y) \tag{3}$$

where the transverse natural mode function $W_k(x, y)$ is calculated using a two-dimensional finite element method for the delta wing plate based on a standard computational code.[10] The in-plane natural mode functions $U_i(x, y)$ and $V_j(x, y)$ are calculated using a three-dimensional finite element method for the delta wing. In this latter computational model, the transverse displacement w is constrained, and only the in-plane mode functions are extracted. These functions satisfy the boundary conditions of the cantilevered delta wing.

For the in-plane equations, it is assumed that all of the nonconservative forces act in the z direction only and the in-plane inertia may be neglected. Thus, the in-plane equations of motion are determined from the stretching strain energy and the Lagrange equation.[1,3,4] The nondimensional in-plane (u and v) equations are then

$$\sum_p C_p^j a_p + \sum_g C_g^j b_g = C^j \tag{4}$$

$$\sum_p D_p^s a_p + \sum_g D_g^s b_g = D^s \tag{5}$$

where C^j and D^s are nonlinear (quadratic) functions of the delta wing transverse deflection.

The transverse equation is formed by substituting the kinetic, bending, and stretching energy expressions into Lagrange's equation. The nondimensional equation is

$$\sum_m A_m^k\left[\ddot{q}_m + 2\omega_m\xi_m\dot{q}_m + \omega_m^2 q_m\right] + \frac{F_N^k}{\tau^2} + \frac{Q^k}{\tau^2} = 0 \tag{6}$$

where A_m^k are constant coefficient terms and F_N^k is a (nondimensional) nonlinear force that depends on the deflection of the plate. Also, ξ_m and ω_m are the mth structural modal damping and natural frequency. Q^k is the nondimensionalized generalized aerodynamic force [see Eq. (10)]. We will discuss it next.

Aerodynamic Equations: Vortex Lattice Model

The flow about the cantilever plate is assumed to be incompressible, inviscid, and irrotational. We use an unsteady vortex lattice method to model this flow. A typical planar vortex lattice mesh for the three-dimensional flow is shown in Fig. 1. The plate and wake are divided into a number of elements. In the wake and on the wing all of the elements are of equal size, Δx, in the streamwise direction. Point vortices are placed on the plate and in the wake at the quarter chord of the elements. At the three-quarter chord of each plate element, a collocation point is placed for the downwash; i.e., we require the velocity induced by the discrete vortices to equal the downwash arising from the unsteady motion of the delta wing. Thus, we have the relationship

$$w_i^{t+1} = \sum_j^{kmm} K_{ij}\Gamma_j^{t+1}, \qquad i = 1, \ldots, km \tag{7}$$

where w_i^{t+1} is the downwash at the ith collocation point at time step $t+1$, Γ_j is the strength of the jth vortex, and K_{ij} is an aerodynamic kernel function.[6] As described in Ref. 6, we have an aerodynamic matrix equation:

$$[A]\{\Gamma\}^{t+1} + [B]\{\Gamma\}^t = \{w\}^{t+1} \tag{8}$$

where $[A]$ and $[B]$ are aerodynamic coefficient matrices.

From the fundamental aerodynamic theory, we can obtain the pressure distribution on the plate at the jth point in terms of the vortex strengths. The nondimensional pressure is given by

$$\overline{\Delta p_j} = \frac{c}{\Delta x}\left[\frac{\Gamma_j^{t+1} + \Gamma_j^t}{2} + \sum_i^j \left(\Gamma_i^{t+1} - \Gamma_i^t\right)\right] \tag{9}$$

and the aerodynamic generalized force is calculated from

$$Q^k = \frac{\rho_\infty U^2 c^4}{Dh}\int_0^1\int_0^1 \overline{\Delta p} W_k \, dx \, dy \tag{10}$$

Aeroelastic State-Space Equations

Consider a discrete time history of the delta wing, $q(t)$, with a constant sampling time step Δt. The structural dynamic equations [Eq. (6)] can be reconstituted as a state-space equation in discrete-time form, i.e.,

$$[D_2]\{\theta\}^{t+1} + [D_1]\{\theta\}^t + [C_2]\{\Gamma\}^{t+1} + [C_1]\{\Gamma\}^t = -\{F_N\}^{t+\frac{1}{2}} \tag{11}$$

where the vector $\{\theta\}$ is the state of the plate, $\{\theta\} = \{\dot{q}, q\}$, and $[D_1]$ and $[D_2]$ are matrices describing the plate structural behavior. $[C_1]$ and $[C_2]$ are matrices describing the vortex element behavior on the delta wing itself.

There is a linear relationship between the downwash w at the collocation points and delta wing response $\{\theta\}$. It is defined by

$$\{w\} = [E]\{\theta\} \tag{12}$$

Thus, by the combination of Eqs. (8), (11), and (12), we obtain a complete aeroelastic state-space equation in matrix form:

$$\begin{bmatrix} A & -E \\ C_2 & D_2 \end{bmatrix}\begin{Bmatrix} \Gamma \\ \theta \end{Bmatrix}^{t+1} + \begin{bmatrix} B & 0 \\ C_1 & D_1 \end{bmatrix}\begin{Bmatrix} \Gamma \\ \theta \end{Bmatrix}^t = \begin{Bmatrix} 0 \\ -F_N \end{Bmatrix}^{t+\frac{1}{2}} \tag{13}$$

Reduced-Order Aerodynamic Model

If we assume the structural response to be zero, then from Eq. (8) we obtain a representation of unforced fluid motion:

$$[A]\{\Gamma\}^{t+1} + [B]\{\Gamma\}^{t} = 0 \tag{14}$$

From Eq. (14), an aerodynamic eigenvalue problem may be formed. Because the matrices $[A]$ and $[B]$ are nonsymmetric, we must compute the right and left eigenvalues and eigenvectors of the generalized eigenvalue problem. They are

$$[A][X][Z] = -[B][X] \tag{15}$$

$$[A]^T[Y][Z] = -[B]^T[Y] \tag{16}$$

where $[Z]$ is a diagonal matrix whose diagonal entries contain the eigenvalues. The discrete time eigenvalues z_i are related to continuous time eigenvalues λ_i by $z_i = \exp(\lambda_i \Delta t)$. The real part of λ_i indicates the aerodynamic modal damping of the system, and the imaginary part of λ_i provides the oscillation frequency.

The right and left eigenvectors are orthogonal with respect to the matrices $[A]$ and $[B]$. We normalize the eigenvectors such that they are orthonormal with respect to A. Therefore,

$$[Y]^T[A][X] = [I] \tag{17}$$

$$[Y]^T[B][X] = -[Z] \tag{18}$$

Next, let the point vortex vector $\{\Gamma\}$ be a linear combination of the R_a right eigenvectors (where usually in practice $R_a \ll$ total number of aerodynamic eigenvalues), i.e.,

$$\{\Gamma\} = [X_{Ra}]\{\gamma\} \tag{19}$$

where $\{\gamma\}$ is the vector of the aerodynamic modal coordinates. Substitution of Eq. (19) into Eq. (8), premultiplication of Eq. (8) by $[Y_{Ra}]^T$, and use of the orthogonality conditions [Eqs. (17) and (18)] yield the new aeroelastic model,

$$\begin{bmatrix} I & -Y_{Ra}^T E \\ C_2 X_{Ra} & D_2 \end{bmatrix} \begin{Bmatrix} \gamma \\ \theta \end{Bmatrix}^{t+1} + \begin{bmatrix} -Z_{Ra} & 0 \\ C_1 X_{Ra} & D_1 \end{bmatrix} \begin{Bmatrix} \gamma \\ \theta \end{Bmatrix}^{t} = \begin{Bmatrix} 0 \\ -F_N \end{Bmatrix}^{t+\frac{1}{2}} \tag{20}$$

We find that, with the reduced-order aerodynamic model, only a few aerodynamic eigenmodes need to be retained in the aeroelastic model for good accuracy. However, although the dominant eigenmodes have been retained, all of the eigenmodes participate in the response to some degree. To account for the neglected eigenmodes, therefore, we use a quasi-static correction that accounts for much of their influence. This technique is similar to the mode-acceleration method common to structural dynamics and was first suggested in the context of fluid eigenmode analysis by Florea and Hall.[11] Finally, the reduced-order model with static correction is given by

$$\begin{bmatrix} I & -Y_{Ra}^T[I - A(A+B)^{-1}]E \\ C_2 X_{Ra} & D_2 + C_2(A+B)^{-1}E \end{bmatrix} \begin{Bmatrix} \gamma_d \\ \theta \end{Bmatrix}^{t+1} + \begin{bmatrix} -Z_{Ra} & -Y_{Ra}^T B(A+B)^{-1}E \\ C_1 X_{Ra} & D_1 + C_1(A+B)^{-1}E \end{bmatrix} \begin{Bmatrix} \gamma_d \\ \theta \end{Bmatrix}^{t} = \begin{Bmatrix} 0 \\ -F_N \end{Bmatrix}^{t+\frac{1}{2}} \tag{21}$$

Numerical Results

Three delta wing configurations of constant 1677-cm^2 platform area with respective leading-edge sweep angles of 30, 45, and 60 deg and corresponding panel aspect ratios of 3.45, 2.00, and 1.15 have been studied. The models were constructed of aluminum alloy plate. The plate thickness for the 30- and 45-deg sweep models was 0.23 cm; the plate thickness for the 60-deg sweep model was 0.16 cm. Poisson's ratio is $\nu = 0.3$. A structural damping ratio of 0.01 was used for all modes.

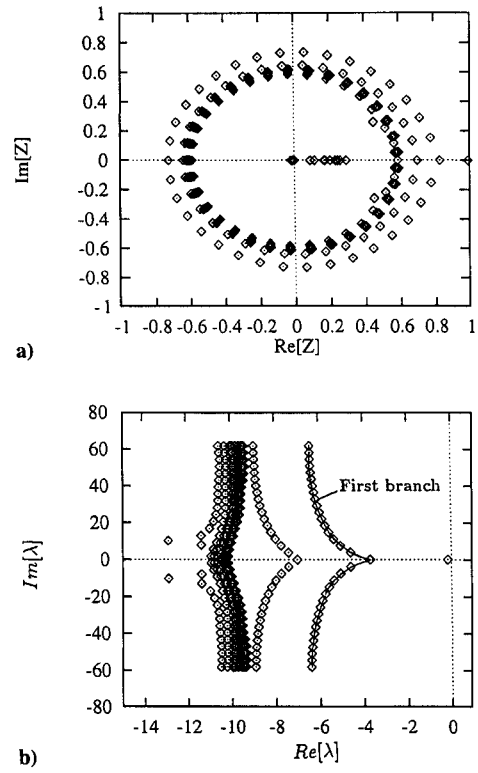

Fig. 2 Eigenvalue solutions of vortex lattice model of unsteady three-dimensional flow about a delta wing: *kn* = 15, *km* = 15, and *kmm* = 50.

For the basic case, the delta wing was modeled using 120 vortex elements, i.e., $km = 15$ and $kn = 15$. The wake was modeled using 525 vortex elements, i.e., $kmm = 50$. The total number of vortex elements (or aerodynamic degrees of freedom) was 645. The nominal delta wing structural modal numbers were $nxy = 5$ in the out-of-plane direction and $mxy = 10$ in the in-plane direction. The vortex relaxation factor was taken to be $\alpha = 0.992$.

Aerodynamic Eigenmodes

The aerodynamic mesh for the delta wing was constructed using a combination of triangular and quadrilateral elements, and the wake mesh was modeled using the quadrilateral element. Typical aerodynamic eigenvalues for the basic vortex lattice model are shown in Fig. 2. Figure 2a shows eigenvalues in terms of the discrete time multiplier z and Fig. 2b in terms of the usual continuous time eigenvalue λ. Note that, for normalization purposes, in presenting these results the airspeed U is assumed to be unity, and thus $\Delta t = \Delta x$. It is found that there are 15 branches in the λ distribution. (Recall that the number of spanwise locations $kn = 15$.) As shown in Ref. 5, we find the first λ branch is the most important. It includes 1 pure real eigenmode and 14 complex conjugate eigenmodes indicated by the solid line and $\Diamond$ symbol in Fig. 2b.

Stability of the Linear Aeroelastic Model

When the nonlinear force F_N in Eq. (13), Eq. (20), or Eq. (21) is set to zero, a linear aeroelastic model is obtained. The aeroelastic eigenvalues obtained from solving these equations determine the stability of the system. When the real part of any one eigenvalue λ becomes positive, the entire system becomes unstable.

Figures 3a and 3b show a typical graphical representation of the eigenanalysis in the form of real eigenvalues $\mathrm{Re}(\lambda_i)$ vs the flow velocity, as well as a root-locus plot for the nominal linear system using all aerodynamic eigenmodes and a reduced-order aerodynamic model for the 60-deg sweep delta wing. There is an intersection of $\mathrm{Re}(\lambda_i)$ with the velocity axis at $U_f = 82.5$ m/s, the critical flutter velocity using all of the aerodynamic modes ($R_a = 645$), with a corresponding flutter oscillatory frequency $\omega_f = 28.5$ Hz, as indicated by the Δ symbol. Using a reduced-order aerodynamic model

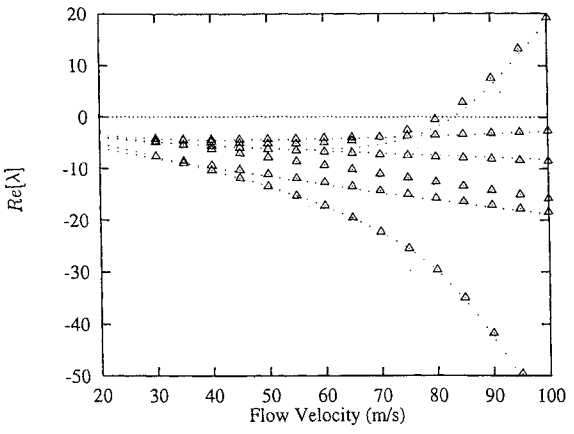

a) Real part

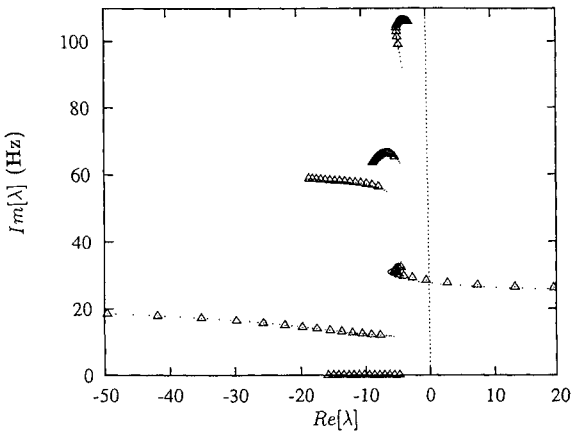

b) Root locus

Fig. 3 Eigenvalue solutions of linear aeroelastic model using all aerodynamic modes and also using a reduced-order aerodynamic model with static correction: $R_a = 9$.

with a static correction and only nine aerodynamic eigenmodes ($R_a = 9$), i.e., the first nine eigenmodes in the first λ branch corresponding to Fig. 2b, the corresponding values are $U_f = 84.5$ m/s and $\omega_f = 27.9$ Hz. These latter results are indicated by the · symbol. The flutter velocity and frequency using the reduced-order aerodynamic model are virtually identical to those from the all-eigenmodes aerodynamic model. However, the computation time using the reduced-order model is only about $\frac{1}{200}$ that of the original model.

Figure 4 shows the flutter velocity and frequency vs different aerodynamic vortex elements. There are four cases to be considered: $km = kn = 5$, $kmm = 20$ [90 degrees of freedom (DOF)]; $km = kn = 10$, $kmm = 40$ (355 DOF); $km = kn = 15$, $kmm = 50$ (645 DOF); and $km = kn = 20$, $kmm = 55$ (910 DOF). As the vortex element increases, the results show good convergence.

For the 30- and 45-deg sweep delta wing models, the flutter velocities and frequencies are $U_f = 74.5$ and 91.1 m/s and the corresponding ω_f are 22.4 and 30.7 Hz, respectively. The first natural torsional frequencies of these models are 42.2 and 54.1 Hz.

To compare the present flutter results to the experimental data in Ref. 8, the results are presented in the form of the flutter velocity index v_I, which is a parameter commonly used to correlate flutter data from different configurations. This nondimensional parameter is defined by the relationship

$$v_I = \frac{U_f}{2\pi f_{\text{ref}} b_{\text{ref}} \sqrt{\mu}}$$

where U_f is the flutter velocity, b_{ref} is a reference length (mean semichord), f_{ref} is a reference frequency (first torsional natural frequency), and μ is the mass ratio parameter, which is defined as the mass of the delta wing divided by the mass of a circumscribed volume of air.[8] The results are shown in Fig. 5. Figure 5a is for the

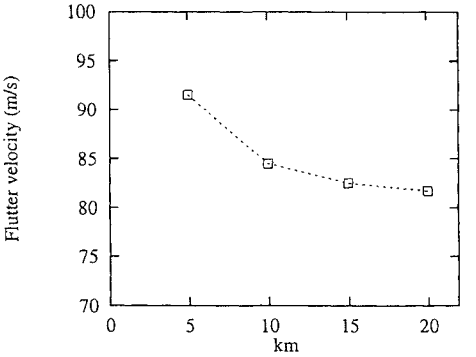

a) For flutter velocity

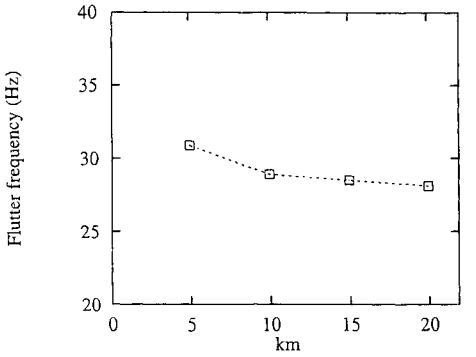

b) For flutter frequency

Fig. 4 Linear flutter characteristics vs the number of aerodynamic vortex elements.

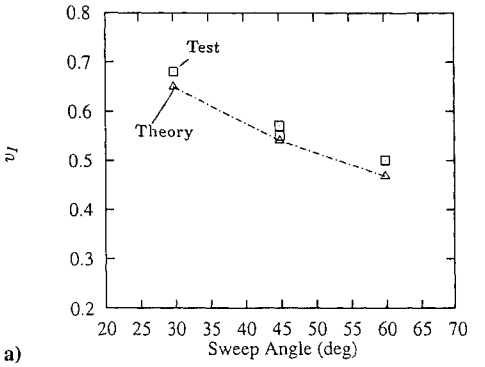

a)

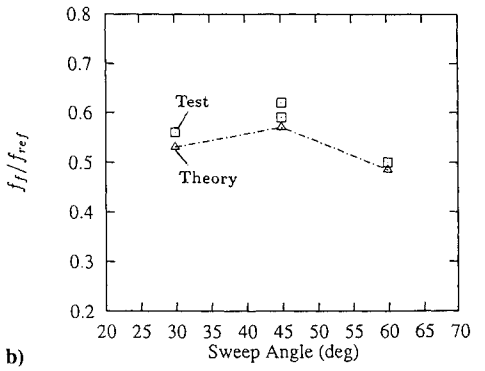

b)

Fig. 5 Variation of flutter velocity index and flutter frequency ratio with sweep angle.

flutter index and Fig. 5b for the flutter frequency. Good agreement is obtained between the present theory and the experimental data of Doggett and Solstmann.[8]

Limit Cycle Oscillation of Nonlinear Model

We have used a standard discrete time algorithm to calculate the nonlinear response of this aeroelastic system using the full aerodynamic model [Eq. (13)] and also the reduced-order aerodynamic model [Eq. (21)]. The time step is constant for a given flow velocity

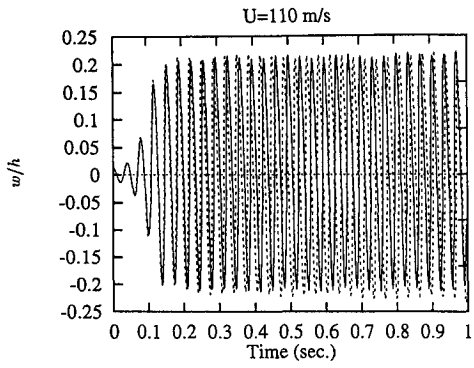

a) For time history

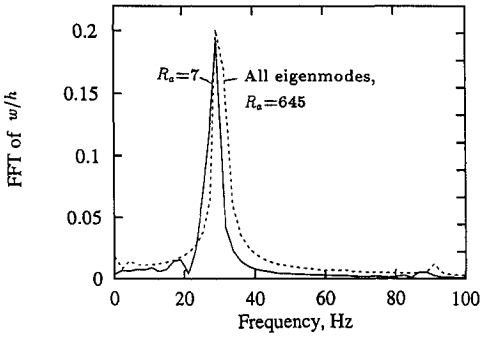

b) For FFT analysis

Fig. 6 LCOs of nondimensional transverse deflection using all aerodynamic eigenmodes and a reduced-order model: $R_a = 7$.

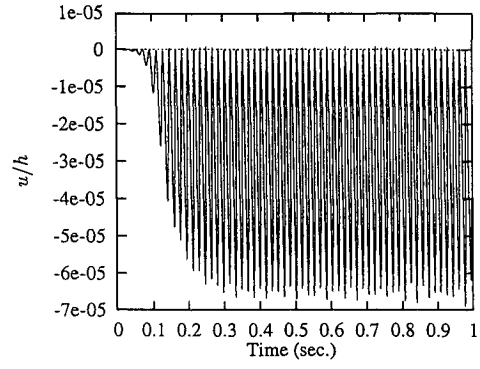

Fig. 7 LCOs of in-plane displacement u using all aerodynamic eigenmodes.

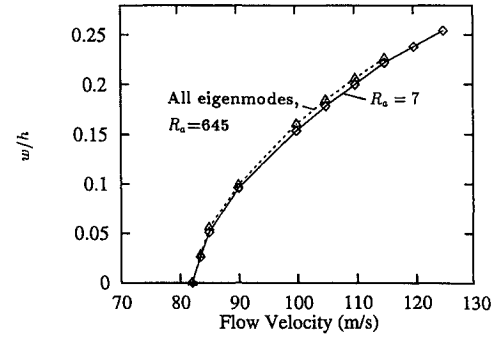

Fig. 8 Limit cycle amplitudes vs flow velocity U using all aerodynamic eigenmodes and a reduced-order model with $R_a = 7$.

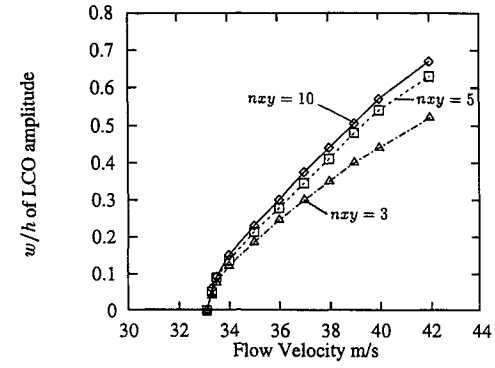

Fig. 9 Theoretical nondimensional transverse peak amplitude vs the flow velocity for several numbers of out-of-plane structural modes and $mxy = 10$.

U, $\Delta t = \Delta x/U$. The results presented are only for the 60-deg sweep delta wing model.

A typical nondimensional transverse displacement time history and corresponding fast Fourier transform (FFT) at location ($x = 1$, $y = 1$) for $U = 110$ m/s $> U_f$ are shown in Figs. 6a and 6b. The dashed line is from using all of the aerodynamic eigenmodes, and the solid line is from the reduced-order aerodynamic model with a static correction for seven aerodynamic eigenmodes ($R_a = 7$). There is a steady-state limit cycle oscillation with dominant frequency of $\omega = 30.7$ Hz. Note that the linear flutter velocity and frequency are $U_f = 82.5$ m/s and $\omega_f = 28.5$ Hz. From Fig. 6, it is seen that, with using only seven aerodynamic eigenmodes ($R_a = 7$), the results are close to those from the all-eigenmodes aerodynamic model for the dominant frequency component with some error for the higher harmonic component.

Typical nondimensional in-plane displacement u time history at location ($x = 1$, $y = 1$) for $U = 110$ m/s $> U_f$ is shown in Fig. 7. The results are from the all-eigenmodes aerodynamic model. Figure 7 reveals that, as the plate deflects in both the positive and negative z direction, the in-plane displacement amplitude, u or v, increases in the negative x or y direction. Thus, the maximum transverse displacements w, both positive and negative, correspond to the maximum negative in-plane displacements, and the in-plane displacements oscillate at twice the transverse oscillation frequency, $\omega = 61.4$ Hz. The point at which the in-plane x displacement is at its smallest amplitude coincides with the point at which the transverse displacement is at its smallest amplitude. Note that, if we were to change the sign of the initial conditions, then Fig. 6a would undergo a sign reversal, but Fig. 7 would be unchanged because u and $v \sim w^2$. Note also that u and $v \ll w$. However, u and v are essential to creating the limit cycle oscillation (LCO) through their nonlinear coupling with w. It can be shown that the strain energy contributions arising from u and v are comparable to those derived from w for the LCO response.

Figure 8 shows the nondimensional transverse rms amplitude of the LCO vs the flow velocity using all ($R_a = 645$) aerodynamic eigenmodes and also the reduced-order model with $R_a = 7$. It is found when only $R_a = 7$ is used that the results are close to those obtained using all of the aerodynamic eigenmodes. Note that, when $U > 115$ m/s, we find a numerical divergence using all ($R_a = 645$) aerodynamic eigenmodes. This is because the time step Δt is not small enough (here Δx is fixed). For the results using the reduced-order model, Δt can be selected to be any value, whatever the Δx of the original aerodynamic model, which is another benefit of using reduced-order analysis. There is no numerical divergence in the higher velocity range using small Δt and the reduced-order model.

To consider the effects of the number of out-of plane modes on the response of the LCO, several numbers of out-of-plane structural modes were used in the calculations, as shown in Fig. 9. Also, the effects of the number of in-plane modes on the response of the LCO were investigated for $nxy = 10$ and $mxy = 5$, 10, 15, and 20. The results are shown in Fig. 10. The transverse LCO amplitude increases as the out-of-plane or in-plane total modal number increases for a given flow velocity. The nominal modal numbers of $nxy = 10$ or $nxy = 5$ and $mxy = 10$ that we used for most of the calculations reported here seem reasonable choices when weighting the balance between computational accuracy and cost. This calculation was for

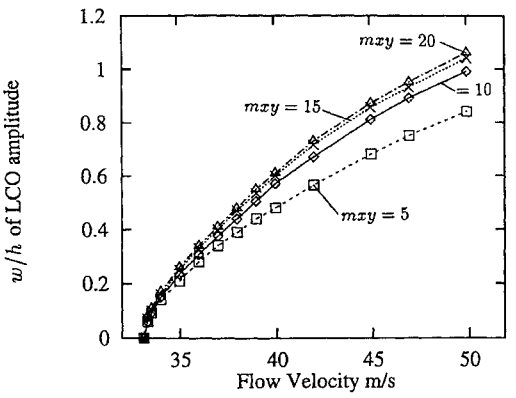

Fig. 10 Theoretical nondimensional transverse peak amplitude vs the flow velocity for several numbers of in-plane structural modes and $nxy = 10$.

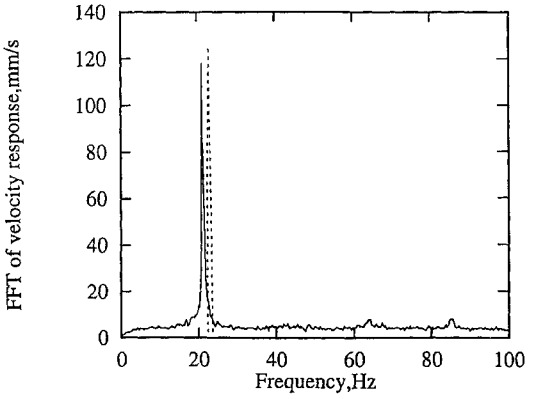

Fig. 11 FFT analysis of theoretical and experimental transverse velocity response located near the tip of delta wing for $U = 45.5$ m/s.

an experimental 0.079-cm-thick aluminum model, as described in the next section.

Experimental Investigation of the LCOs

Description of Experiment

The experimental model is a simple delta wing configuration with a leading-edge sweep of 45 deg. The model was constructed from a 0.24-cm-thick plastic (Lucite® material) plate. The root chord was locally clamped (cantilevered), and the length of the cantilever root was 23 cm (60% root chord). The clamping was symmetric about the center of the root chord of the model. The length of the root chord was 38.1 cm. The clamped root of this model is fixed on a root support mechanism, which is placed at the top of the tunnel. The delta wing model is mounted in a vertical position in the center of the test section that eliminates gravitational preload in the out-of-plane direction. To avoid the effect of the wind-tunnel body vibration on the model response, the root support mechanism of the model was separated from the ceiling of the tunnel. The mechanism is directly mounted to a heavy support frame, which is supported to the ground.

Structural response measurements were made using the Ometron VPI 4000 scanning laser vibrometer system.[9] The VPI sensor is a noncontacting transducer that uses optical interferometry and electronic frequency measurements to determine the frequency shift of a beam of light reflected from a moving surface. The system then uses frequency tracking methods to convert the frequency shift to an analog voltage corresponding to the velocity of the moving surface. Because there is no contact between the laser and the delta wing, the system is capable of making point velocity FFT or power spectrum measurements without altering the dynamics of the delta wing or the flow across it.

Correlation Between Theoretical and Experimental Results

The theoretical prediction is based on Eq. (21). We use the aerodynamic vortex lattice model including 120 vortex elements on the delta wing ($km = kn = 15$) and 525 vortex elements in the wake ($kmm = 50$) and 9 reduced aerodynamic eigenmodes, $R_a = 9$. The delta wing structural modal numbers were $nxy = 10$ in the out-of-plane and $mxy = 10$ in the in-plane directions, respectively. The mesh of the finite element model for the out-of-plane structural model is 30×30, and thus, the delta wing was modeled using 900 quadrilateral plate elements. The mesh of the three-dimensional finite element model for the in-plane structural model is $30 \times 30 \times 1$, and the delta wing was modeled using 961 solid elements with 1921 nodes. The nodes at the clamped root chord satisfy geometric boundary conditions, i.e., $w = u = v = R_x = R_y = R_z = 0$.

The theoretical first 10 natural frequencies (hertz) are 7.47, 29.61, 33.84, 70.27, 83.78, 107.01, 132.95, 143.91, 153.67, and 180.58, and the experimental first five natural frequencies are 7.5, 29.25, 35.25, 71.35, and 85.50. The agreement is good.

The theoretical flutter velocity of this model is 40.25 m/s, and the corresponding flutter frequency ω_F is 21.25 Hz.

Figure 11 shows a typical experimental FFT analysis of the transverse velocity response at the measurement point located near the tip of delta wing for $U = 45.5$ m/s. The LCO is dominated by a 23.0-Hz harmonic frequency component. The background aerodynamic noise has a random characteristic. For comparison, a theoretical FFT is also plotted, as shown in a broken line. It is found that the theoretical LCO is a one harmonic motion and coincides closely with the experimental result.

Figure 12 shows a three-dimensional FFT analysis of the experimental data for several flow velocities from 36.3 to 45.5 m/s. It is very clear that at the flow velocities lower than the flutter velocity (40.25 m/s) the structural response has a broad frequency band with a small amplitude. This response is because of the turbulence in the wind tunnel. At flow velocities higher than the flutter velocity, the structural response has an LCO characteristic that is dominated by one harmonic frequency component. The LCO amplitude increases with increasing flow velocity.

As shown in Fig. 11, the measured velocity response is not a pure harmonic motion; therefore, we use an average rms method to characterize the response for correlation purposes. The sampling rate is 500 point/s, $\Delta t = \frac{1}{500}$, and total sampling length is 10,000 points. The measured rms velocity $\dot{w}_{\text{rms}}$ is determined from these data. In the present experiment, the measured rms velocity is normalized by $h\omega_F$.

Figures 13a and 13b show the theoretical and experimental nondimensional transverse rms velocity amplitude (Fig. 13a) and frequency (Fig. 13b) of the LCO vs the flow velocity at the measurement point located near the tip of delta wing. In general, the agreement is good.

To consider the effects of the plate thickness on the experimental results, a delta wing plate model constructed from a 0.079-cm-thick aluminum alloy sheet was also tested. The other parameters of the model were the same as described earlier for the plastic model. The theoretical flutter velocity of this model is 33.1 m/s, and the corresponding flutter frequency is $\omega_F = 24.5$ Hz. Figures 14a and 14b show the theoretical and experimental nondimensional transverse rms velocity amplitude (Fig. 14a) and frequency (Fig. 14b) vs the flow velocity at the measurement point located near the tip of delta wing. In general, the agreement is not as good as for the plastic model, and there is a consistently larger error between theory and experiment in the range of higher flow velocities both for the amplitude and frequency of the LCO. This difference is likely due to the unavoidable initial plate curvature of this very thin aluminum plate. Recently completed calculations by the present authors for a curved delta wing model (to be reported separately) have confirmed this effect.

Figure 15 shows the vibration shape of the thin aluminum model during LCO and the correlation between theoretical and experimental nondimensional transverse rms velocity amplitude at $U = 36.4$ m/s. The agreement is reasonably good.

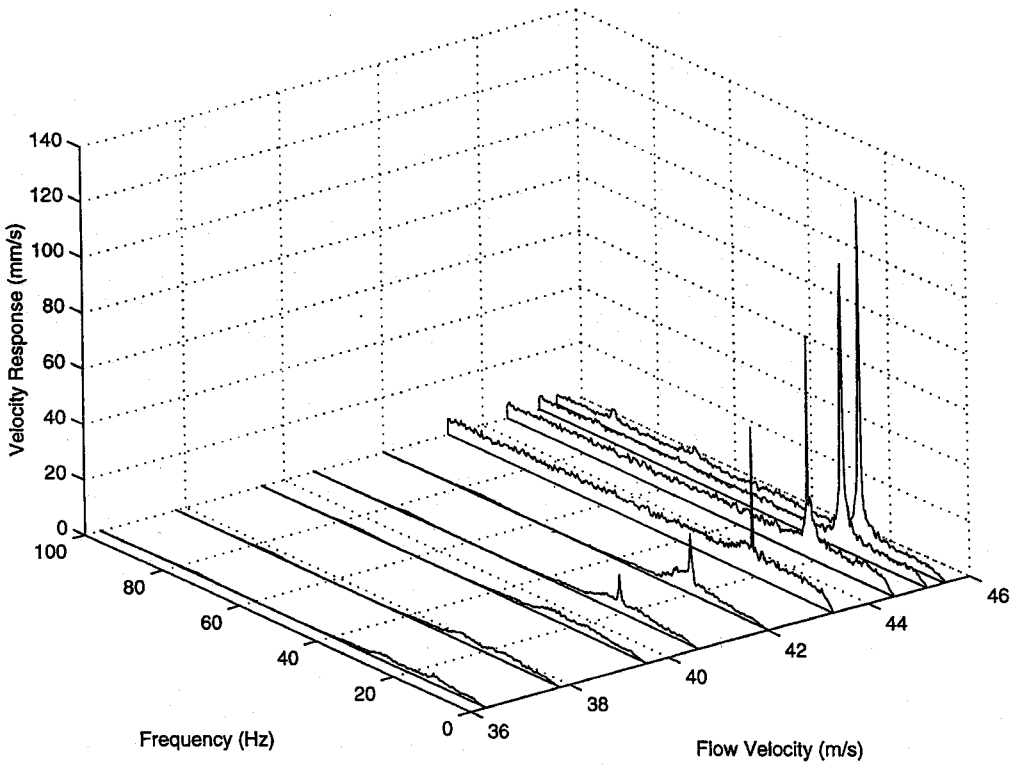

Fig. 12 Waterfall of FFT analysis vs flow velocity.

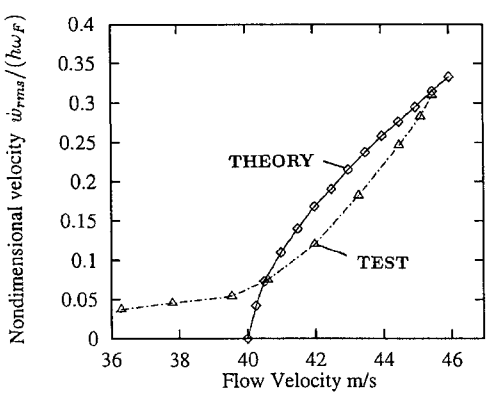

a) Theoretical and experimental nondimensional transverse velocity $\dot{w}_{\rm rms}/(h\omega_F)$

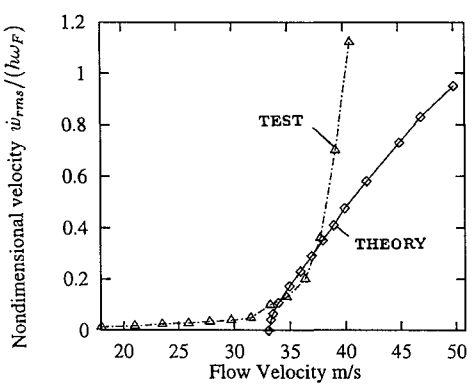

a) Theoretical and experimental nondimensional transverse velocity $\dot{w}_{\rm rms}/(h\omega_F)$

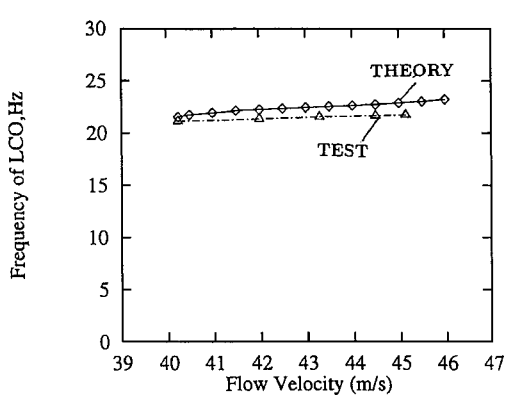

b) Frequency

Fig. 13 LCO vs flow velocity (plastic wing model).

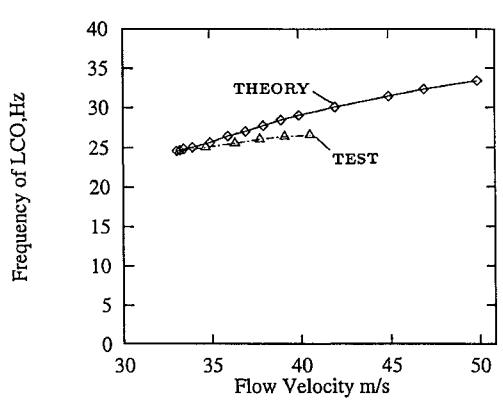

b) Frequency

Fig. 14 LCO vs flow velocity (very thin aluminium model).

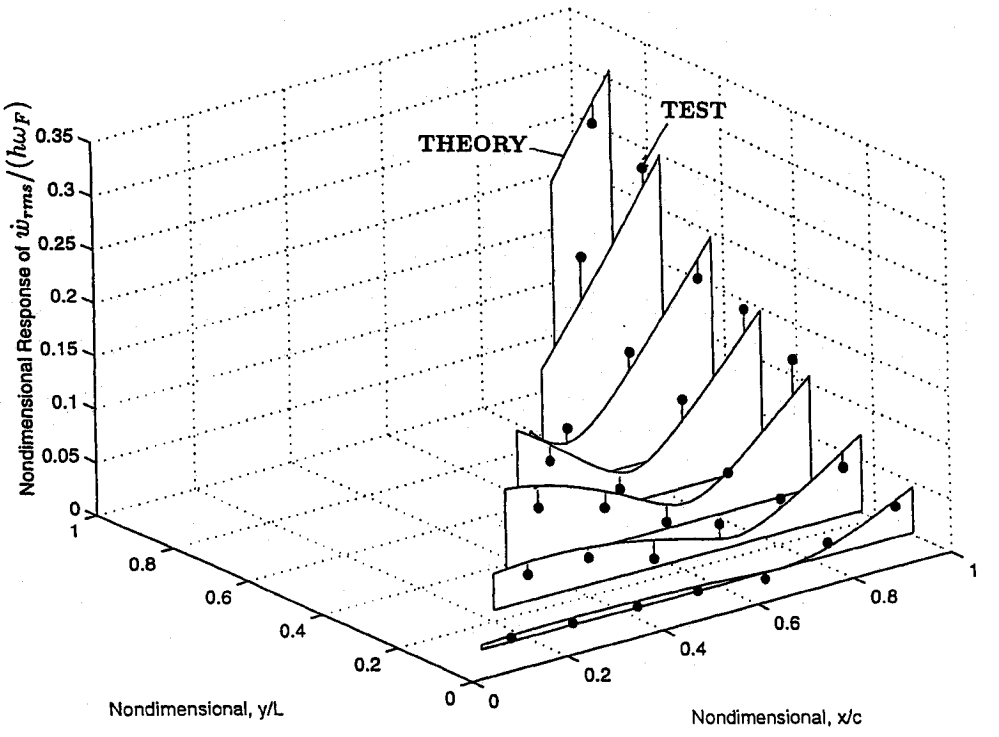

Fig. 15 Vibration shape and correlation between theoretical and experimental nondimensional transverse velocity amplitude (very thin, aluminum model).

Conclusion

Vortex lattice aerodynamic theory has been used to construct a reduced-order aerodynamic model that has been successfully applied to determine the nonlinear limit cycle response of simple delta wing models. It was shown that the unsteady three-dimensional flow can be modeled accurately using a few aerodynamic eigenmodes plus a static correction technique and, thus, can be easily coupled to a structural system for nonlinear aeroelastic analysis. Reduced-order aerodynamic and structural models are used to substantially decrease computational cost with no loss in accuracy. Without the use of reduced-order models, calculations of the LCO would be impractical. The theoretical results for the flutter boundary (beyond which LCO occurs) have been validated by comparison to the experimental data reported by other earlier investigators for low-aspect-ratio delta wings. Also, the LCOs found experimentally in the present study are consistent with the theoretical results.

The present paper provides new insight into a nonlinear aeroelastic phenomena not previously widely appreciated, i.e., LCO for low-aspect-ratio wings that have a platelike structural behavior. This adds to our understanding of nonlinear aeroelastic wing theory.

Acknowledgments

This work was supported under U.S. Air Force Office of Scientific Research Grant "Limit Cycle Oscillations and Nonlinear Aeroelastic Wing Response." C. I. Chang and Brian Sanders are the grant program officers. The authors would also like to thank Robert Clark for his help with implementing the laser measurement system. All numerical calculations were done on a supercomputer, T916, in the North Carolina Supercomputing Center.

References

[1]Dowell, E. H., *Aeroelasticity of Plates and Shells*, Kluwer, Dordrecht, The Netherlands, 1975, pp. 35–44.

[2]Ricketts, R. H., Noll, T. E., Whitlow, W., Jr., and Huttsell, L. J., "An Overview of Aeroelasticity Studies for the National Aero-Space Plane," AIAA Paper 93-1313, April 1993.

[3]Hopkins, M. A., and Dowell, E. H., "Limited Amplitude Panel Flutter with a Temperature Differential," AIAA Paper 94-1486, April 1994.

[4]Weiliang, Y., and Dowell, E. H., "Limit Cycle Oscillation of a Fluttering Cantilever Plate," *AIAA Journal*, Vol. 29, No. 11, 1991, pp. 1929–1936.

[5]Tang, D., Dowell, E. H., and Hall, K. C., "Limit Cycle Oscillations of a Cantilevered Wing in Low Subsonic Flow," *AIAA Journal*, Vol. 37, No. 3, 1999, pp. 364–371.

[6]Hall, K. C., "Eigenanalysis of Unsteady Flows About Airfoils, Cascades, and Wings," *AIAA Journal*, Vol. 32, No. 12, 1994, pp. 2426–2432.

[7]Dowell, E. H., "Eigenmode Analysis in Unsteady Aerodynamics: Reduced-Order Models," *AIAA Journal*, Vol. 34, No. 8, 1996, pp. 1578–1588.

[8]Doggett, R. V., and Solstmann, D. L., "Some Low-Speed Flutter Characteristics of Simple Low-Aspect-Ratio Delta Wing Models," NASA TM 101547, Jan. 1989.

[9]*VPI 4000 Scanning Laser Vibrometer Operator's Manual*, Ometron, Inc., Sterling, VA, Oct. 1997.

[10]Wilson, E. L., *Structural Analysis Programs 90, Version 5.10, Reference Manual*, Computers and Structures, Inc., Berkeley, CA, June 1983.

[11]Florea, R., and Hall, K. C., "Reduced Order Modeling of Unsteady Flows About Airfoils," *Aeroelasticity and Fluid Structure Interaction Problems*, edited by P. P. Friedmann and J. C. J. Chang, AD-Vol. 44, American Society of Mechanical Engineers, New York, 1994, pp. 49–68.

A. Chattopadhyay
Associate Editor